ERDC/CHL CHETN-I-XX
April 2024

US Army Corps of Engineers®

US Army Corps of Engineers (USACE) Wave Information Study: 2021 Annual Update

by Candice Hall, Robert E. Jensen, Clarence O. Collins, Tyler J. Hesser, and Mitchell E. Brown

PURPOSE: This Coastal and Hydraulics Engineering Technical Note (CHETN) describes the 2021 Wave Information Study (WIS) annual update. Within this CHETN, we summarize the WIS input data, explain the model technologies, detail the quality control / quality assurance (QA/QC), and provide statistical evaluation of the 2021 WIS estimates as compared to in situ buoys and remotely sensed satellite altimeter data.

INTRODUCTION: The WIS project provides a national resource of long-term wave climatologies for all US coastal waters. WIS uses third generation phase-averaged wave models forced with high-resolution wind fields and mean daily ice concentration fields. The outputs are extensively evaluated to ensure high-quality wave estimates. This multidecade hindcast and storm event archive is generated to meet a wide array of coastal engineering needs.

For the WIS 2021 annual update, all WIS basins, except for the Great Lakes Region, use the European Centre for Medium-Range Weather Forecasts (ECMWF) ERA5 reanalysis monthly wind and ice files (Hersbach et al. 2019); for the Great Lakes Region, the Climate Forecast System Reanalysis (CFSR) database is used (Saha et al. 2010, 2014). The wind fields are enhanced by embedding all tropical cyclones and the top 10 storm events using kinematic procedures on extratropical storms (Cox et al. 1995). The WIS 2021 annual update used two wave modeling technologies: The Wave Model (WAM) and WAVEWATCH III® (WW3; Komen et al. 1994; Tolman 2009).

The WIS 2021 hindcast shows good statistical agreement at available point-source-measurement evaluation sites, with domain-wide bias statistics of 0.1 meters (m), 0.1 seconds (s), and −2.5° and root-mean-square errors (RMSEs) of 0.3 m, 1.5 s, and 64° for significant wave height (H_{m0}), mean wave period (T_m), and mean wave direction defined at the spectral peak frequency (α_p), respectively. Pearson correlations for all three wave parameters remain above 70% across the domains. Evaluations against satellite altimeter for H_{m0} show a total bias of −0.06 m, a total RMSE of 0.43 m, and a total correlation of 0.91; maps of bias and RMSE show good agreement along the US continental seaboards and island territories.

Because the level of performance was acceptable, the WIS 2021 wave estimates augmented the WIS hindcast archive, and WIS products generated from these new estimates are available via the interactive WIS Portal (*https://wisportal.erdc.dren.mil/*) and the Portal Application Programming Interface (API; *https://wisportal.erdc.dren.mil/wis-api/apidocs*). The full historical WIS hindcast (1980 to 2021) and the full historical US Army Corps of Engineers (USACE) Quality Controlled and Consistent Measurement Archive (Hall and Jensen 2021, 2022) used during WIS evaluations are available on the Coastal and Hydraulics Laboratory (CHL) Data Server (*https://chldata.erdc.dren.mil/thredds/catalog/catalog.html*). For more information on the WIS program, please see the WIS website (USACE 2023; *https://wis.erdc.dren.mil*).

WIS 2021 EVALUATION RESULTS

Comparison to Point-Source Measurements: The following WIS wave spectral parameters are considered: significant wave height (H_{m0}), mean wave period (T_m), mean wave direction defined at the spectral peak frequency (α_p), wind speed, and wind direction. WIS estimates are compared with available point-source measurements from NOAA's National Data Buoy Center (NDBC), Fisheries and Oceans Canada's Marine Environmental Data Section (MEDS), and the Scripps Institution of Oceanography (SIO) Coastal Data Information Program (CDIP). The NDBC wave sensor accuracy limits ($H_{m0} = \pm 0.2$ m, $T_m = \pm 1$ s, $\alpha_p = \pm 10°$, wind speed = ±1.0 m/s, and wind direction = $\alpha_p = \pm 10°$) are used as evaluation standards within this work (NDBC 2023). Appendix A contains an overview of the WIS 2021 modeling technologies, operations, input files, evaluation procedures, and statistical equations.

The quality or deficiency in modeled wave conditions is highly dependent on the quality of the wind measurement forcing. Notably, H_{m0} scales to the square of the wind speed. Therefore, it is critical to evaluate the point-source measurements and modeled wind speed and direction to provide insights into the wave estimates. However, these point-source measurements are discrete subsamples in time and space of a wind field that can be 100s of kilometers in radial coverage for extratropical weather systems. Additionally, the measured wind speeds are adjusted for elevation and stability to match the modeled 10 m equivalent neutral, stable wind. Moreover, not all wave measuring buoys are equipped with wind sensors. These evaluations are important, but they will not answer all of the uncertainty associated with the complete description of a spatially and temporally variable meteorological system.

Overall, WIS 2021 wave products show good statistical agreement (Table 1) across the WIS 2021 evaluation sites for the wave parameters, H_{m0}, T_m, and α_p, and for wind speed and wind direction. In the case of a nested grid, model results are based on the output from only the highest resolution grid in the simulation, so there is no redundancy in the analysis. Approximately 212 buoy sites were used in the evaluation.

For H_{m0}, the models perform well, with bias between 0.23 m (Alaska) and 0.014 m (Atlantic Ocean), indicating that the model is underestimating wave height. RMSE values range from 0.53 m (Alaska) to 0.26 m (Atlantic Ocean). Pearson correlation generally falls above 0.90, with mean absolute error (MAE) and relative standard error (RSE) following similar tendencies. The models tend to underestimate T_m, with an upper bias of 1.6 s (Pacific Ocean), with the remaining domains hovering around 1 s. T_m RMSE values range from 1 s to a high of 2.6 s (Pacific Ocean). Correlation is lower for T_m than for H_{m0}, as are MAE and RSE. For α_p, bias is around 10°, indicating a slight rotational difference from the point-source measurements, where negative values are shifted clockwise and positive values are shifted counterclockwise. With observed point-source-measurement variation or standard deviation about the mean, retuned RMSEs of 50° to 60° are reasonable (NDBC 2023). Even for the Great Lakes, which are known for rapid cyclogenesis and shifting directions, being 90° out of phase is not that large and may be attributed to poor wind forcing. Correlation values are low compared to H_{m0} or T_m, but as shown in the scatter plot in Figure 1, model estimates are consistent.

Wind speed biases are low and fall below 1 m/s, with overestimation of the models within Alaska, Atlantic Ocean, and Gulf of Mexico and underestimation within the Pacific Ocean and Great Lakes (Table 1). The scatter (i.e., RMSE) is approximately 1.5 to 3 m/s. Correlation values run low because winds are notably temporally variable, which does not translate within the modeled winds. MAE and RSE results follow the RMSE ranges (Table 1). The wind direction bias echoes α_p: all negative (i.e., shifted clockwise) and ranging from 1.5° to 23° (Great Lakes), suggesting that the wind field

specification also lacks the variability observed at individual in situ sites. The remaining RMSE, correlation, MAE, and RSE reiterate the α_p results (Table 1).

Table 1. Wave Information Study (WIS) 2021 domain-specific statistical results.

Variable	Domain	*n*	Bias	RMSE	Correlation (*r*)	Mean Absolute Error (MAE)	Residual Standard Error (RSE)
Significant Wave Heights (m)	Alaska	126,509	0.233	0.535	0.952	0.370	0.409
	Atlantic Ocean	395,927	0.014	0.257	0.945	0.184	0.249
	Gulf of Mexico	109,255	0.138	0.239	0.943	0.176	0.186
	Pacific Ocean	691,499	0.088	0.397	0.945	0.273	0.348
	Great Lakes	137,499	0.029	0.226	0.891	0.155	0.224
Mean Wave Period (s)	Alaska	126,509	1.151	1.596	0.759	1.252	1.054
	Atlantic Ocean	386,016	1.126	1.482	0.805	1.237	0.851
	Gulf of Mexico	109,255	0.774	0.977	0.820	0.816	0.524
	Pacific Ocean	691,499	1.698	2.399	0.613	1.866	1.452
	Great Lakes	54,596	0.725	0.928	0.832	0.787	0.576
Mean Wave Direction (˚)	Alaska	113,557	−11.151	50.218	0.750	23.077	44.535
	Atlantic Ocean	367,288	4.173	59.141	0.721	24.403	52.682
	Gulf of Mexico	109,243	5.172	58.862	0.730	26.449	54.216
	Pacific Ocean	618,381	−1.093	51.904	0.818	23.007	49.219
	Great Lakes	84,752	−9.501	99.782	0.547	55.927	87.803
Wind Speed (m/s)	Alaska	104,148	−0.732	2.944	0.785	1.740	2.451
	Atlantic Ocean	220,676	−0.162	1.858	0.842	1.152	1.680
	Gulf of Mexico	72,103	−0.180	1.412	0.869	0.957	1.246
	Pacific Ocean	329,104	0.064	2.355	0.806	1.439	2.099
	Great Lakes	131,220	0.174	2.241	0.729	1.612	2.054
Wind Direction (˚)	Alaska	89,204	−3.019	65.754	0.747	27.511	60.927
	Atlantic Ocean	197,410	−2.617	63.764	0.803	25.846	59.995
	Gulf of Mexico	54,238	−1.502	55.832	0.790	21.462	52.428
	Pacific Ocean	319,201	−11.222	73.800	0.754	31.722	67.966
	Great Lakes	130,797	−21.284	107.177	0.519	57.917	83.635

Scatterplots visually represent the 2021 bulk wave parameters (H_{m0}, T_m, and α_p) for each point-source-measurement site. Figure 1 and Figure 2 display the monthly mean (left panels) for the time-paired H_{m0}, T_m, α_p, wind speed, and direction model versus point-source measurements. To capture top events that exceeded the 90th percentile, a second scatterplot (right panels) was generated for the top

90th percentile monthly mean of each parameter. The mean monthly 90th percentile directions are those associated with the existing H_{m0} and wind speed, respectively. In all plots, symbols indicate above or below the 200 m isobaths, while colors delineate regional domains. Linear fit and locally weighted scatterplot smoothing (LOWESS) curves, a line of perfect fit, and the number of samples (*n*) are included within each plot.

The monthly mean H_{m0} results (Figure 1, top left panel) show strong similarity to the point-source measurements for the wave height range. The distribution of the results for each of the five WIS domains isolates wave climate variations, where the Great Lakes (magenta symbols) occupy the lower end of the range, the Gulf of Mexico (green symbols) is slightly higher, and the Atlantic (blue symbols) and Alaska (dark blue symbols) are even higher. However, the Pacific covers the entire range (orange symbols). All domain-specific results yield similar results for quality, with a limited number of outliers that are generally from the Pacific domain. At the upper limit, there is a tendency for the model to underestimate H_{m0}, which is indicative of both the linear fit and LOWESS being located below the line of perfect fit. This occurs at about 2 m, increasing with H_{m0}. However, the departure from the perfect fit is less than 0.5 m. The scatter in the model estimates is about 0.25 m for all domains and follows the statistics in Table 1. The monthly mean 90th percentile H_{m0} evaluations (Figure 1, top right panel) are similar in structure to the mean monthly scatterplot. However, the range is shifted upward to a maximum of about 9 m. The linear and LOWESS lines are nearly identical, although both depart further from the line of perfect fit, indicating the model is underestimating the highest conditions in a given month.

The mean monthly T_m results (Figure 1, middle left panel) clearly illustrate the variation in the wave climates for the five WIS domains. Overall, the models underestimate the point-source measurements in all domains and are comparable to the bias values found in Table 1. From the LOWESS, the bias for all domains hovers around 1 s for the range in T_m values. Scatter is relatively contained, excluding the outliers, to about 1 s, with the exception of a cluster of sites in the Pacific domain. Those sites are from the Southern California Bight region, where this evaluation had to use Level 3 WIS wave estimates for comparison. (Appendix A contains domain-level explanations.) Note that WIS estimates for these sites within the WIS Data Portal are extracted from updated Level 4 wave model results. The mean monthly 90th percentile (Figure 1, middle right panel) complements the overall mean monthly graphic. The model T_m estimates are biased low for a range of conditions, along with a scatter around 1 s.

The lower panels in Figure 1 display the α_p results for the mean monthly (left) and mean 90th percentile (right) comparisons between the model and point-source measurements. Based on the linear fit and LOWESS, there is consistency over the full directional range for the model to approximate the point-source measurements. Scatter exists, but this is likely due to the dependency in α_p to the peak frequency, which is variable in measured α_p during cyclogenesis and due to orographic effects found in the Great Lakes, the wind-sea swell systems in the Atlantic, and the complex island sheltering in the Pacific. This peak-frequency-dependent variability likely introduces a temporal mismatch between observations and model estimates. Unlike the consistency between the overall mean and mean monthly 90th percentile results of H_{m0} and T_m, there is a broader scatter for α_p, especially for the Atlantic domain during the transition from locally generated wind-seas to swells. There is also a departure of the linear fit and LOWESS from the line of perfect fit when compared to the overall mean (Figure 1, lower left panel).

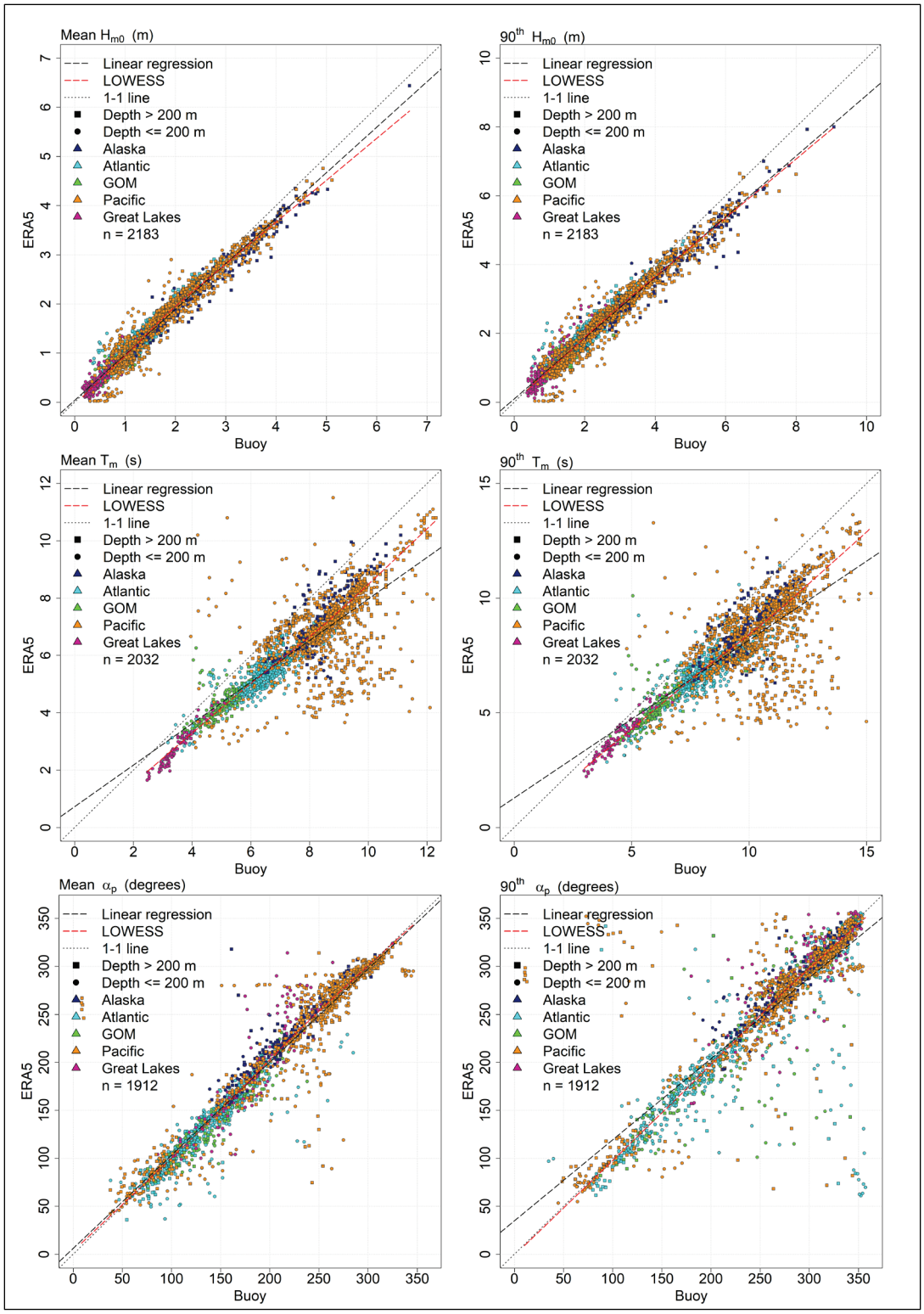

Figure 1. Mean (*left*) and top 90th percentile (*right*) for significant wave height (*top*), mean wave period (*middle*), and wave direction at peak frequency (*bottom*) between WIS 2021 and point-source measurements.

Figure 2 displays the mean monthly (left panels), mean 90th percentile (right panel), wind speed (top panels), and wind direction (bottom panels) for the point-source measurements used in the evaluation.

The mean monthly wind speed plot (Figure 2, upper left panel) shows good agreement between the modeled and wind point-source measurements (range of 2.5 to 10 m/s), although the model estimates fall below the line of perfect fit. Scatter of the central data points is limited to 2 m/s, consistent with the RMSE values found in Table 1. Outliers exist (e.g., the vertical line between 0 and 5 m/s), and a cluster of points to the right of the line of perfect fit indicates an overestimation in the modeled winds. The LOWESS falls along the line of perfect fit, but it is controlled by the temporally mismatched estimates, as previously mentioned, while the linear fit reflects both sets of outliers more than the bulk of the data points. The mean monthly 90th percentile (Figure 2, top right panel) is similar in structure to the mean monthly scatterplot. However, the range increases to a maximum of about 20 m/s. Similar outliers exist below the line of perfect fit. Again, LOWESS falls slightly below the line of perfect fit until 5 m/s, from where the poorly modeled wind estimates are indicated by a horizontal LOWESS. Linear fit is again more heavily influenced by the outlier points than by the bulk of the data. Scatter appears to be slightly elevated compared to the monthly mean.

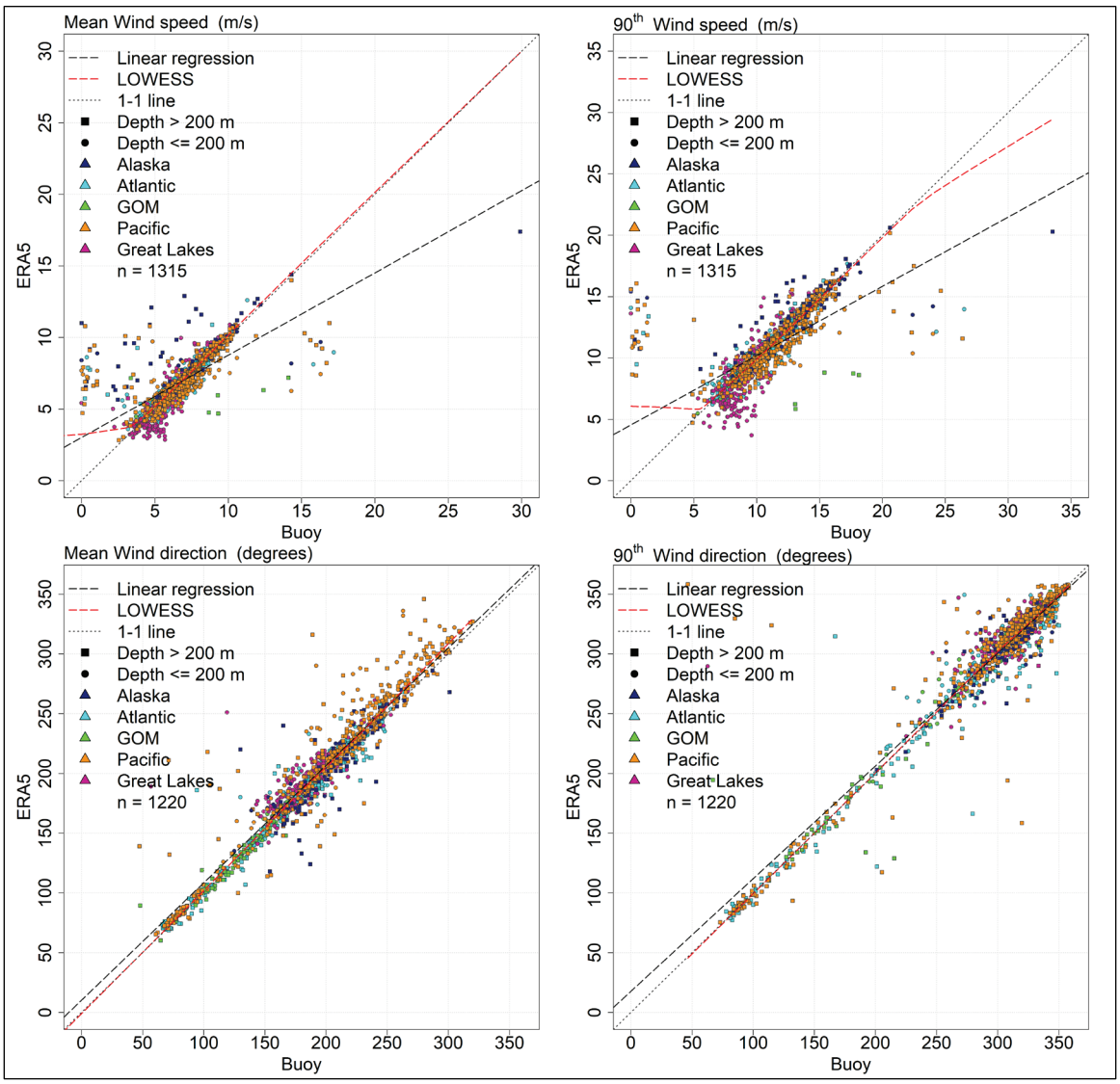

Figure 2. Mean (*left*) and top 90th percentile (*right*) for wind speed (*top*) and direction (*bottom*) between WIS 2021 and point-source measurements.

The comparison of mean monthly wind direction (Figure 2, lower left panel) shows good agreement across all five WIS domains and directions. The distribution of the points is weighted slightly below the line of perfect fit, reflecting a clockwise rotational shift in the model estimates (negative bias in Table 1). The LOWESS follows the line of perfect fit, although there is a slight deviation in the linear fit. The scatter in results varies for the directional range and domain, where the Gulf of Mexico has the least scatter, and the Pacific and Great Lakes have the greatest (Figure 2, lower left panel), which complements the statistics in Table 1. The mean monthly 90th percentile wind direction (Figure 2, lower right panel) shows distinct separation in the five WIS regions. The Pacific and Alaska fall in the range of wind directions from 250° to 350°, reflecting the westerly component of the winds, while the Atlantic, Gulf of Mexico, and Great Lakes are dominated by easterly to southerly winds (90° to 180°). There is a significant increase in scatter, especially below the line of perfect fit, from the Atlantic and Gulf of Mexico sites that is similar to the α_p results (Figure 1, lower right panel). LOWESS follows the line of perfect fit, while the linear fit falls above it until about 225° and then falls below the line of perfect fit (Figure 2, lower left panel).

While the statistics and scatterplots provide an overview of the quality of the WIS 2021 hindcast, it is equally important to identify site-specific quality or deficiency in the model runs. Figure 3 presents the H_{m0} RMSE statistic in map view for each point-source-measurement site. The legend is graduated from light (0.1 to 0.3 m) to dark (>1.5 m), so the lighter the color, the lower the RMSE. For the Atlantic, Gulf of Mexico, and Great Lakes regions, RMSEs are generally less than 0.3 m for all sites (Figure 3). The Pacific and Alaska RMSE values are generally less than 0.3 m for the offshore sites and increase to 0.5 m for the coastal buoys. Elevated RMSEs exist for about five locations that are in complex coastal areas and are generally in the lee of offshore islands. The combined H_{m0} correlation for all sites within each WIS domain (Table 1) ranges from about 0.9 to 0.95. However, the individual-sites map in Figure 4 shows areas requiring improvement. The Atlantic, Gulf of Mexico, Great Lakes, Alaska, and most sites in the Pacific return high correlation values. Poor (less than 0.3) correlation exists for many of the sites in the Southern California Bight, where as previously noted, lower resolution model estimates were used in the evaluation.

A similar analysis is performed for T_m, where RMSE and correlation (Figure 5 and Figure 6, respectively) are presented. Overall RMSE ranged from 0.9 s (Great Lakes) to 2.4 s (Pacific), while the correlation ranged from 0.6 (Pacific) to 0.8 (Great Lakes). There are a significant number of temporally mismatched estimates in the overall mean monthly and mean 90th percentile model estimates compared to the point-source measurements (Figure 1, middle panels). Figure 5 illustrates exactly where those deficiencies exist. There is relatively good agreement, or low RMSE values, in the Atlantic, Gulf of Mexico, Great Lakes, and most of the Pacific coastal sites to the north of the Southern California Bight, including the Hawaiian Islands. All sites in the Southern California Bight contain elevated RMSE values of 4 s or greater because the evaluations are using lower resolution model results accompanied with lower resolution wind fields.

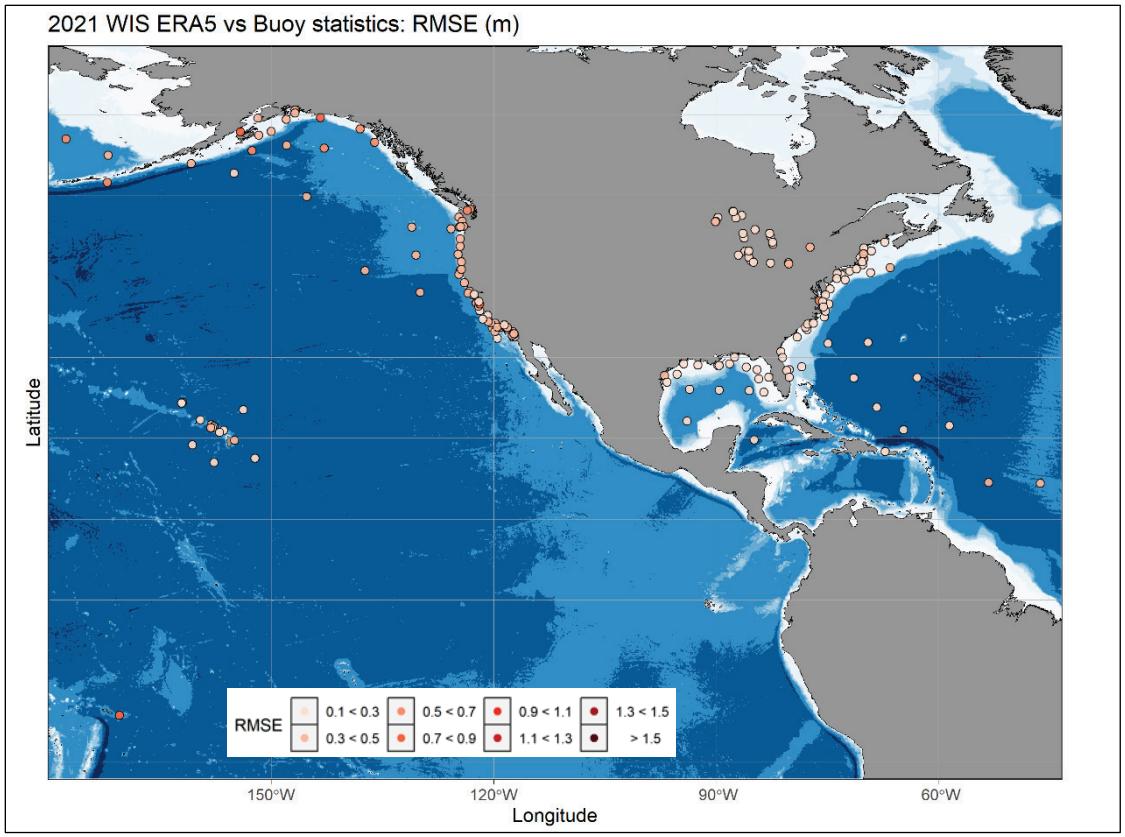

Figure 3. Site-specific, significant wave height root-mean-square error (RMSE) between WIS 2021 and point-source measurements.

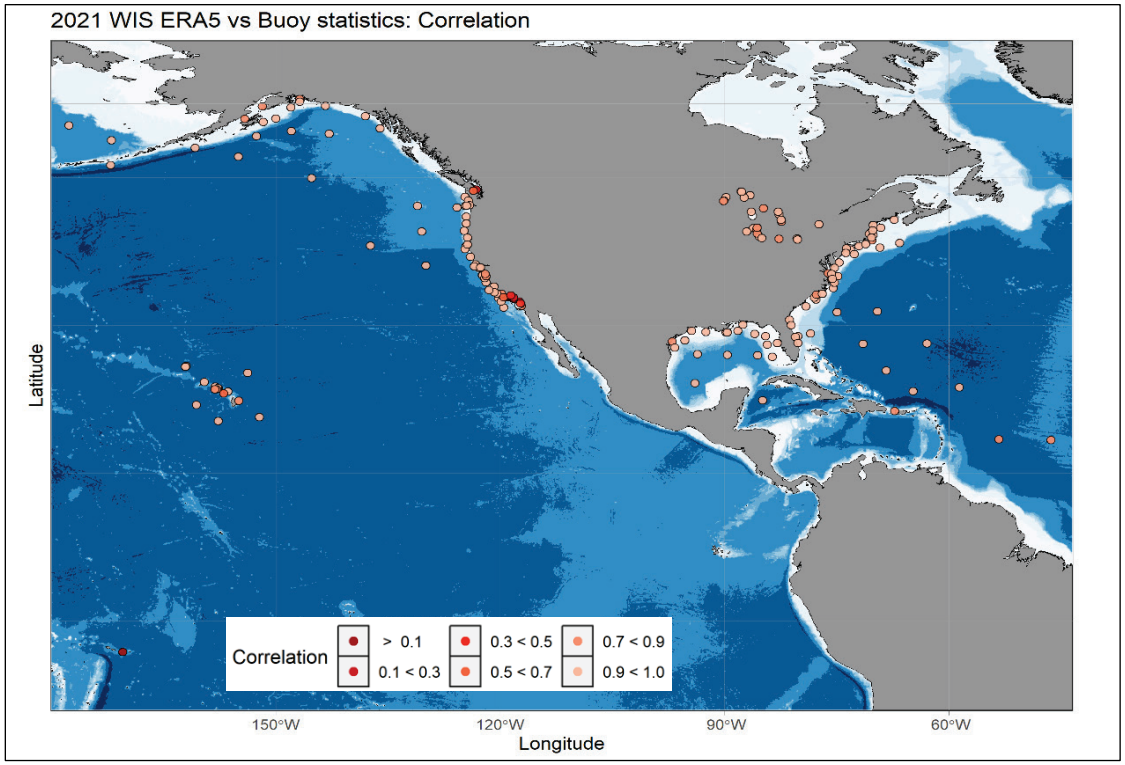

Figure 4. Site-specific significant wave height correlations between WIS 2021 and point-source measurements.

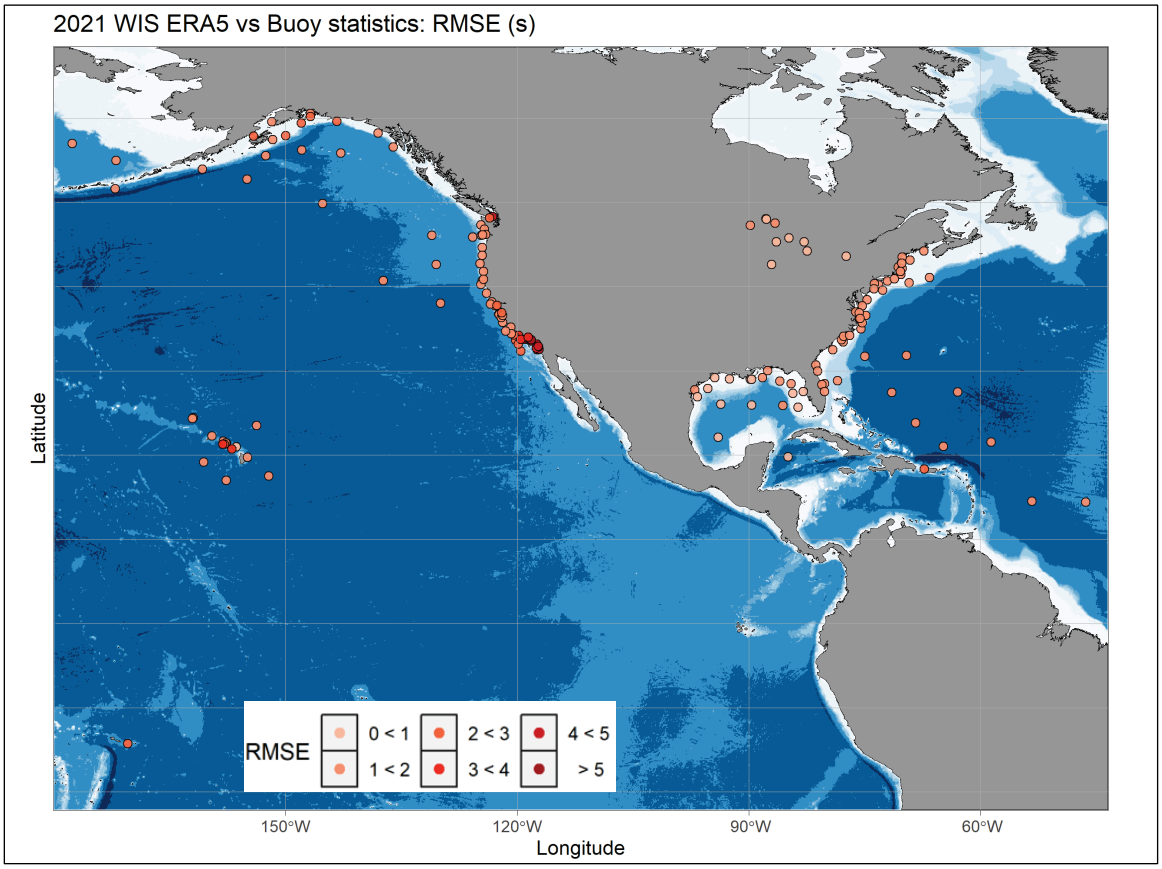

Figure 5. Site-specific mean wave period RMSE between WIS 2021 and point-source measurements.

Correlation values above 0.8 exist for all but two sites in the Atlantic (Figure 6), in the strongly sheltered region around Cape Cod. The Gulf of Mexico, Great Lakes, and Alaska generally contain correlation values in the 0.8 range (Figure 6). The Pacific is slightly more complicated. The majority of the Pacific offshore sites, including the coastal sites north of San Francisco and the Hawaiian Islands, return values of 0.8. Deficiencies exist in the landward of islands (e.g., Kodiak Island in the Gulf of Alaska and two sites in the Strait of Juan de Fuca) and again in the Southern California Bight. For more evaluation plots, please see Appendix B, which contains two example WIS 2021 individual site evaluation plots. For the full suite of 2021 individual evaluation plots, please contact *WISinfo@usace.army.mil*.

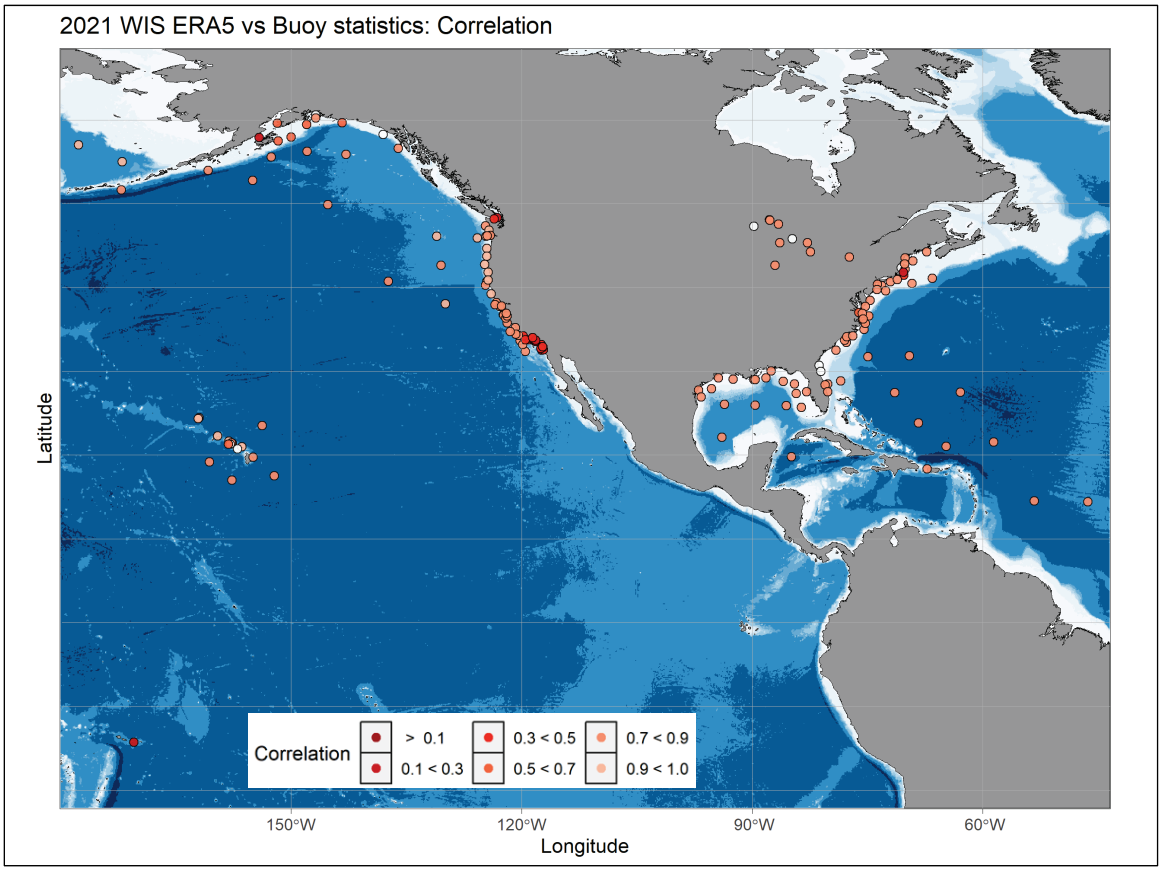

Figure 6. Site-specific mean wave period correlations between WIS 2021 and point-source measurements.

Comparison to Satellite Altimeter: For satellite altimeter WIS evaluation methodologies, please see Appendix A. Table 2 shows the statistical comparison of the Level 1 significant wave height for the WIS 2021 update and the satellite altimeter data. The results are consistent with the evaluations against buoy data. Overall bias is not represented here because the model is known to underpredict wave height along the inactive boundaries in the Level 1 grids and to skew the results. Matching the pattern in the buoy evaluation, the RMSE is lowest in the Gulf of Mexico, the Atlantic, and the Pacific, and it is highest in Alaska. Correlation is high (>0.90) in every domain except the Gulf of Mexico.

Table 2. Grid-specific comparison to altimeter data.

Domain	*n*	RMSE (m)	Correlation (*r*)
Atlantic	22,175,431	0.39	0.92
Gulf of Mexico	491,534	0.35	0.73
Pacific	91,474,196	0.44	0.90
Alaska	2,489,131	0.52	0.93

Figure 7 shows the bias map for the Atlantic Level 1 grid. There is strong negative bias in the extreme northern and southern boundaries. This reflects the lack of active boundaries in these locales. There is high bias around the Windward Islands. There is generally low bias, especially around the US eastern seaboard, but the bias tends to increase toward the eastern part of the basin. There is high

RMSE in the extreme northern and southern boundaries, as expected, and also around the Windward Islands. There is generally low RMSE in the southern portion of the domain and higher RMSE in the northern portion of the domain. There is a pattern of increased RMSE that matches the location of the Gulf Stream extension, which is an area of high extratropical cyclogenesis (Lodise et al. 2022).

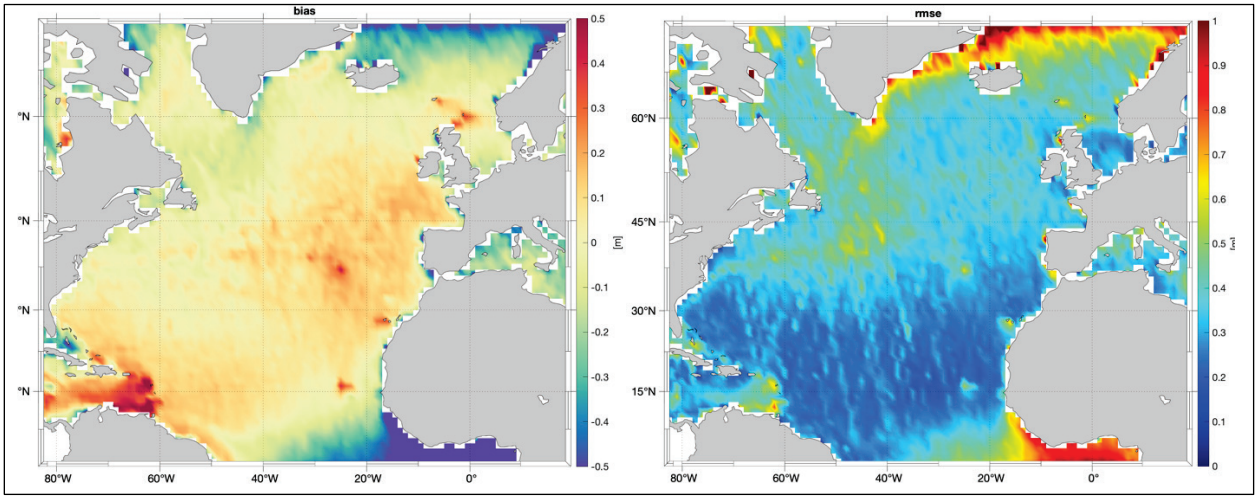

Figure 7. Bias (meters) on the *left* and RMSE (meters) on the *right* for the Atlantic Level 1 grid as evaluated against satellite altimeter data and gridded into 1° bins.

Figure 8 shows the bias map for the Gulf of Mexico Level 2 grid. There is strong negative bias near some land boundaries (e.g., western Cuba, the Yucatan, and southern Louisiana). Otherwise, the bias is slightly negative throughout the Gulf of Mexico. The RMSE map shows areas of high RMSE corresponding to areas of increased bias and generally low RMSE elsewhere, except for a slight increase in the vicinity of the Loop Current and the beginning of the Florida Current.

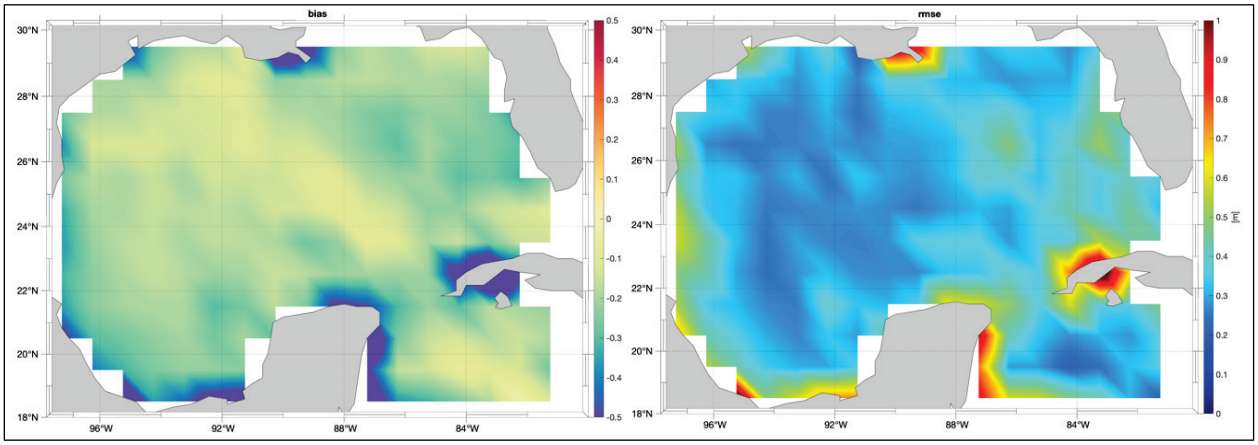

Figure 8. Bias (meters) on the *left* and RMSE (meters) on the *right* for the Gulf of Mexico Level 2 grid, as evaluated against satellite altimeter data and gridded into 1° bins.

Figure 9 shows the bias map for the Pacific Level 1 grid. There is strong negative bias in the extreme west and south of Australia. This reflects the lack of active boundaries. Southern Ocean storms track from west to east, so there is less of a bias issue on the eastern portion of the basin. There is some negative bias to the south of the Hawaiian Island chain, but there is little bias to the north. There are areas of low bias near land boundaries, particularly in the western and northern portions of the basin. There are areas of slight positive bias toward the eastern portion of the basin and around the

Intertropical Convergence Zone. The western seaboard generally shows very low bias. RMSE reflects areas of high bias. Besides western and southern Australia, the Kamchatka Peninsula and the Aleutian chain are areas of increased bias. The midlatitudes show very small RMSE, which increases toward the north and south; this matches the distribution of wave heights: higher wave heights on average in the high-mid to high latitudes and lower wave heights on average in the tropics.

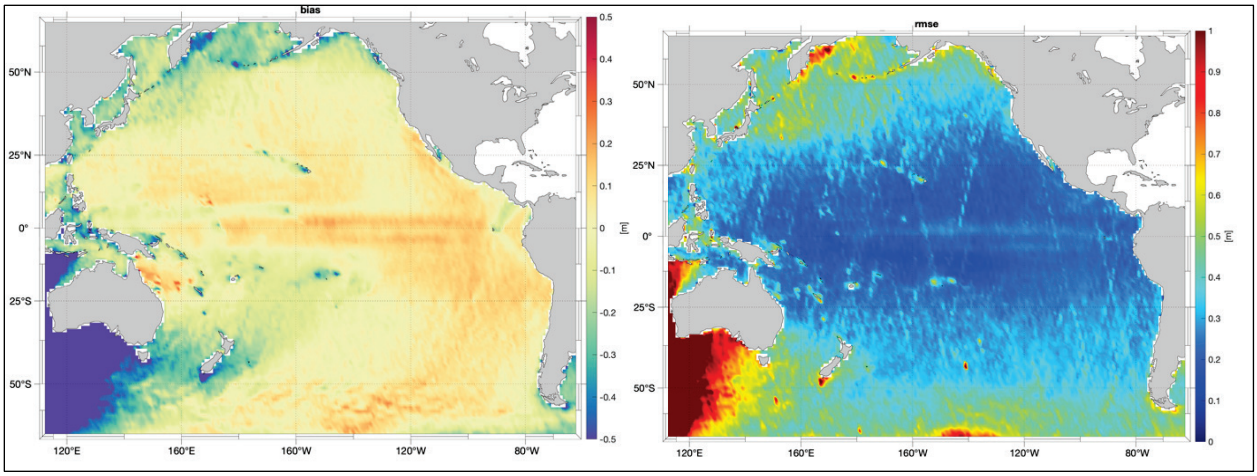

Figure 9. Bias (meters) on the *left* and RMSE (meters) on the *right* for the Pacific Level 1 grid as evaluated against satellite altimeter data and gridded into 1° bins.

Figure 10 shows the bias map for the Alaska Level 2 grid. There is strong negative bias dotted along the Aleutian chain. The bias is generally negative south of the Bering Strait; the eastern portion of the Bering Sea shows positive bias increasing with latitude. There are localized areas of high RMSE throughout the domain (e.g., along the Aleutian chain, along land boundaries, and in the northern portion of the domain). There is low to moderate RMSE in the Bering Sea, just west of northern Alaska and south of the Bering Strait.

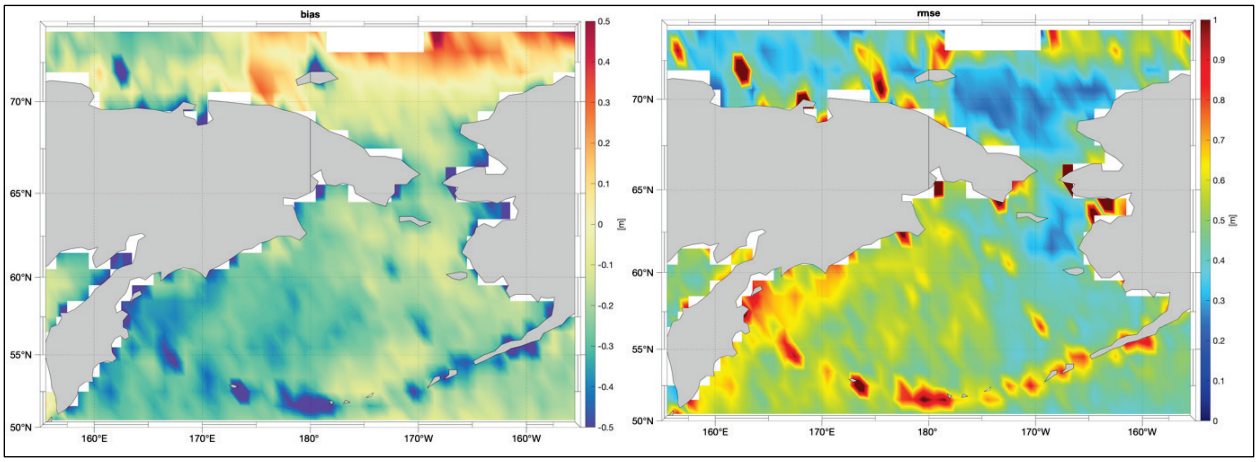

Figure 10. Bias (meters) on the *left* and RMSE (meters) on the *right* for the Alaska Level 2 grid as evaluated against satellite altimeter data and gridded into 1° bins.

CONCLUSION: Averaging across the domains shows that WIS wave estimates perform well against point-source measurements for reviewed variables in all domains and against satellite altimeter data for H_{m0} (Table 3). Using the NDBC accuracy standards (NDBC 2023), paired WIS H_{m0} bias and RMSE across all basins (n = 1,460,689) fall within and near the ±0.2 m range, allowing for elevated

RMSEs that are observed in complex coastal areas and the lee of offshore islands. Bias and RMSE fall close to the NDBC T_m accuracy of ±1 s, although overall Pearson correlations are lower due to a few strongly sheltered sites in the Atlantic (around Cape Cod) and Pacific Oceans (Kodiak Island in the Gulf of Alaska, two sites in the Strait of Juan de Fuca, and in the Southern California Bight). Finally, α_p bias for all domains falls well within the NDBC ±10° standard for direction, with RMSE and Pearson correlation results mirroring both the temporally mismatched estimates and the site-specific discussions previously presented.

Table 3. Overall WIS 2021 point-source measurement statistical results.

Variable	*n*	Bias	RMSE	Correlation
Significant Wave Heights (m)	1,460,689	−0.10	0.33	0.94
Mean Wave Period (s)	1,367,875	−1.09	1.48	0.77
Mean Wave Direction (˚)	1,293,221	2.48	63.98	0.71

The maps of bias and RMSE for H_{m0} revealed that the best performance was generally near the coasts in the areas of interests: along the US eastern and western seaboard and Hawaiian Islands. Poor performance was usually connected to (1) lack of active boundaries, (2) decreased altimeter data quality around island chains, (3) areas of high wave–current interaction, and (4) areas known to be prone to strong extratropical cyclones. All of these issues are areas where model performance improvement is needed in the future. Overall, the comparison was very favorable, with the combined bias of 0.06 m, combined RMSE 0.43 m, and combined correlation of 0.91.

DATA ACCESSIBILITY: The WIS 2021 wave estimates and products are available via the interactive WIS Portal (*https://wisportal.erdc.dren.mil/*) or Portal API (*https://wisportal.erdc.dren.mil/wis-api/apidocs*). The full historical WIS hindcast (1980–2021) and the full historical USACE Quality Controlled and Consistent Measurement Archive used within these evaluations (Hall and Jensen 2021, 2022) are available on the CHL Data Server (*https://chldata.erdc.dren.mil/thredds/catalog/catalog.html*). For more information on the WIS program, please see the WIS website (USACE 2023; *https://wis.erdc.dren.mil*).

ADDITIONAL INFORMATION: This CHETN was prepared, as part of the USACE Coastal and Ocean Data System (CODS) program, by Drs. Candice Hall, Robert E. Jensen, Clarence O. Collins, Tyler J. Hesser, and Mr. Mitchell E. Brown, US Army Engineer Research and Development Center, Coastal and Hydraulics Laboratory, Coastal Processes Branch, Vicksburg, Mississippi. Questions pertaining to this CHETN may be directed to Dr. Candice Hall (*candice.hall@usace.army.mil*) or to the USACE CODS program manager, Dr. Spicer A. Bak.

This CHETN should be cited as follows:

> Hall, C., R. E. Jensen, C. O. Collins, T. J. Hesser, and M. E. Brown. 2024. *US Army Corps of Engineers (USACE) Wave Information Study: 2021 Annual Update.* ERDC/CHL CHETN-I-??. Vicksburg, MS: US Army Engineer Research and Development Center, Coastal and Hydraulics Laboratory. DOI: Insert before publication.

REFERENCES

Ardhuin, F., E. Rogers, A. V. Babanin, J.-F. Filipot, R. Magne, A. Roland, A. van der Westhuysen, et al. 2010. "Semiempirical Dissipation Source Functions for Ocean Waves. Part I: Definition, Calibration, and Validation." *Journal of Physical Oceanography* 40 (9): 917–1,941. https://doi.org/10.1175/2010JPO4324.1.

Battjes, J. A., and J. P. F. M. Janssen. 1978. "Energy Loss and Set-Up Due to Breaking of Random Waves." In *Proceedings, 16th International Conference on Coastal Engineering*, 27 August–3 September, Hamburg, Germany, 569–587, Reston, VA: ASCE. https://doi.org/10.1061/9780872621909.034.

Collins, C. O., and T. J. Hesser. 2021. *altWIZ: A System for Satellite Radar Altimeter Evaluation of Modeled Wave Heights*. ERDC/CHL CHETN-IV-127. Vicksburg, MS: US Army Engineer Research and Development Center, Coastal and Hydraulics Laboratory. https://dx.doi.org/10.21079/11681/39699.

Cox, A. T., J. A. Greenwood, V. J. Cardone, and V. R. Swail. 1995. "An Interactive Objective Kinematic Analysis System." In *Proceedings, 4th International Workshop on Wave Hindcasting and Forecasting*, Banff, Alberta, Canada, 109–118.

GEBCO (General Bathymetric Chart of the Oceans). 2003. General Bathymetric Chart of the Oceans, Centenary Edition [Database]. https://www.gebco.net/.

Hall, C., and R. E. Jensen. 2021. *Utilizing Data from the NOAA National Data Buoy Center*. ERDC/CHL CHETN-I-100. Vicksburg, MS: US Army Engineer Research and Development Center, Coastal and Hydraulics Laboratory. http://dx.doi.org/10.21079/11681/40059.

Hall, C., and R. E. Jensen. 2022. "USACE Coastal and Hydraulics Laboratory Quality Controlled, Consistent Measurement Archive." *Scientific Data* 9 (1): 248. https://doi.org/10.1038/s41597-022-01344-z.

Hasselmann, S., K. Hasselmann, J. H. Allender, and T. P. Barnett. 1985. "Computations and Parameterizations of the Nonlinear Energy Transfer in a Gravity Wave Spectrum. Part II: Parameterizations of the Nonlinear Transfer for Application in Wave Models." *Journal of Physical Oceanography* 15 (11): 1,378–1,391.

Hersbach, H., B. Pell, P. Berrisford, S. Hirahara, A. Horányi, J. Muñoz-Sabater, J. Nicolas, et al. 2019. "The ERA5 Global Reanalysis." *Quarterly Journal of the Royal Meteorological Society* 146 (730): 1,999–2,049. https://doi.org/10.1002/qj.3803.

Hirahara, S., M. Alonso-Balmaseda, E. de Boisseson, and H. Hersbach. 2016. *Sea Surface Temperature and Sea Ice Concentration for ERA5*. ERA Report Series. Berkshire, England: European Centre for Medium Range Weather Forecasts. https://www.ecmwf.int/en/elibrary/79624-sea-surface-temperature-and-sea-ice-concentration-era5.

IPET (Interagency Performance Evaluation Task Force). 2009. *Performance Evaluation of the New Orleans and Southeast Louisiana Hurricane Protection System*. Washington, DC: Department of the Army, US Army Corps of Engineers. https://biotech.law.lsu.edu/katrina/ipet/Volume%20I%20FINAL%2023Jun09%20mh.pdf.

Komen, G. J., L. Cavaleri, M. Donelan, K. Hasselmann, S. Hasselmann, and P. A. E. M. Janssen. 1996. *Dynamics and Modelling of Ocean Waves*. Cambridge, UK: Cambridge University Press.

Lodise, J., S. Merrifield, C. Collins, P. Rogowski, J. Behrens, and E. Terrill. 2022. "Global Climatology of Extratropical Cyclones from a New Tracking Approach and Associated Wave Heights from Satellite Radar Altimeter." *Journal of Geophysical Research: Oceans* 127 (11): e2022JC018925. https://doi.org/10.1029/2022jc018925.

National Centers for Environmental Information. n.d. GEOphysical Data System [Database]. Accessed July 22, 2022. https://www.ncei.noaa.gov/products/marine-trackline-geophysical-data.

National Centers for Environmental Information. n.d. Great Lakes Bathymetry [Database]. Accessed July 22, 2022. https://www.ncei.noaa.gov/products/great-lakes-bathymetry.

NDBC (National Data Buoy Center). 2023. "What Are the Sensor Reporting, Sampling, and Accuracy Readings?" *NOAA NWS NDBC*. https://www.ndbc.noaa.gov/faq/rsa.shtml.

Ortiz-Royero, J. C., and A. Mercado-Irizarry. 2008. "An Intercomparison of SWAN and WAVEWATCH III Models with Data from NDBC-NOAA Buoys at Oceanic Scales." *Coastal Engineering Journal* 50 (1): 47–73. https://doi.org/10.1142/S0578563408001739.

Reguero, B. G., M. Menéndez, F. J. Méndez, R. Mínguez, and I. J. Losada. 2012. "A Global Ocean Wave (GOW) Calibrated Reanalysis from 1948 Onwards." *Coastal Engineering* 65: 38–55. https://doi.org/10.1016/j.coastaleng.2012.03.003.

Ribal, A., and I. R. Young. 2019. "33 Years of Globally Calibrated Wave Height and Wind Speed Data Based on Altimeter Observations." *Scientific Data* 6 (1): 77. https://doi.org/10.1038/s41597-019-0083-9.

Rusu, L., and C. Guedes Soares. 2012. "Wave Energy Assessments in the Azores Islands." *Renewable Energy* 45: 183–196. https://doi.org/10.1016/j.renene.2012.02.027.

Saha, S., S. Moorthi, H.-L. Pan, X. Wu, J. Wang, S. Nadiga, P. Tripp, et al. 2010. "The NCEP Climate Forecast System Reanalysis." *Bulletin of the American Meteorological Society* 91 (8): 1,015–1,058. https://doi.org/10.1175/2010BAMS3001.1.

Saha, S., S. Moorthi, X. Wu, J. Wang, S. Nadiga, P. Tripp, D. Behringer, et al. 2014. "The NCEP Climate Forecast System Version 2." *Journal of Climate* 27 (6): 2,185–2,208. https://doi.org/10.1175/JCLI-D-12-00823.1.

Stopa, J. E., and K. F. Cheung. 2014. "Intercomparison of Wind and Wave Data from the ECMWF Reanalysis Interim and the NCEP Climate Forecast System Reanalysis." *Ocean Modelling* 75: 65–83. https://doi.org/10.1016/j.ocemod.2013.12.006.

Stopa, J. E., and A. Mouche. 2017. "Significant Wave Heights from Sentinel-1 SAR: Validation and Applications." *Journal of Geophysical Research*: *Oceans* 122 (3): 1,827–1,848. https://doi.org/10.1002/2016JC012364.

Tolman, H. L. 2009. *User Manual and System Documentation of WAVEWATCH III TM version 3.14*. Technical Note, MMAB Contribution No. 276. Camp Springs, MD: NOAA. https://polar.ncep.noaa.gov/mmab/papers/tn276/MMAB_276.pdf.

USACE (US Army Corps of Engineers). 2023. "Wave Information Study." https://wis.erdc.dren.mil/index.html.

Van Nieuwkoop, J. C. C., H. C. M. Smith, G. H. Smith, and L. Johanning. 2013. "Wave Resource Assessment Along the Cornish Coast (UK) from a 23-Year Hindcast Dataset Validated against Buoy Measurements." *Renewable Energy* 58: 1–14. http://dx.doi.org/10.1016/j.renene.2013.02.033.

Yang, T.-Y., J. Kessler, L. Mason, P. Y. Chu, and J. Wang. 2020. "A Consistent Great Lakes Ice Cover Digital Data Set for Winters 1973–2019." *Scientific Data* 7 (259). https://doi.org/10.1038/s41597-020-00603-1.

APPENDIX A: WIS 2021 ANNUAL UPDATE—MODELING TECHNOLOGIES, OPERATIONS, INPUTS, AND EVALUATION PROCEDURES

WIS MODELING TECHNOLOGIES: WIS uses 2 third generation phase-averaged wave modeling technologies: WW3 (Tolman 2009) for the Atlantic and Pacific domains and WAM (Komen et al. 1994) for the Gulf of Mexico, Western Alaska, and Great Lakes domains. Two models were used due to varying capabilities, as determined by a three year period of record model evaluation that was performed for each domain (unpublished manuscript, Jensen and Hesser 2005). WAM was chosen for the Gulf of Mexico based on an Interagency Performance Evaluation Task Force (IPET 2009) study (of Hurricane Katrina) and for the Western Alaska and Great Lakes domains because, at that time, only WAM had ice-field implementation. WW3 was selected for the Atlantic and Pacific because results demonstrated the transition of locally generated wind-seas to swell for northeasters and preserved the contribution of distant swell energy, respectively.

The WIS 2021 annual update uses WAM version 4.5.1C, where a cap to the drag coefficient is set, limiting added energy for high wind speeds (unpublished manuscript, Jensen 2006).

Gulf of Mexico: For the Gulf of Mexico, 28 frequency bands characterize the frequency spectra, where each frequency is defined as $f(n) = 1.1 \cdot f(n-1)$, where $f(1) = 0.0314$ Hz. The number of direction bands used is 72 at a resolution of 5°, with a starting direction band of 2.5°.

Western Alaska: For Alaska, the number of frequency and direction bands are 28 and 24, respectively. The frequency range and interval are the same as noted for the Gulf of Mexico. The first directional band is 7.5°, and the remaining bands are set at 15°. Two levels are used in the implementation of WAM for Western Alaska: a 1.0° resolution for Level 1 and a 0.25° resolution for Level 2 domains.

Great Lakes: For the Great Lakes simulations, the number of frequency and directional bands set for each individual lake (i.e., Ontario, Erie, Huron, Michigan, and Superior) are 28 and 72, respectively. The first frequency band for the Great Lakes simulations is set at 0.0611 Hz and follows $f(n) = 1.1 \cdot f(n-1)$. Each lake is run independently from the other lakes. Initial evaluations by Robert E. Jensen in 2011 showed that Lake Ontario and Lake Erie bulk wave parameter results were consistently biased low. Wind-field analyses were performed and compared to shore-based meteorological sites. From a quantile–quantile evaluation, the wind speeds were adjusted. The modification reduced the negative biases found, improving the WIS results for the two lakes. No adjustments were made to the wind fields for Lakes Huron, Michigan, or Superior.

The WIS 2021 annual update uses WW3 version 4.18. For both the Atlantic and Pacific Ocean domains, the model options are identical to the propagation scheme (i.e., 3rd Order, Ultimate Quickest; Tolman, 1995) source term specification: the ST4 Package (Ardhuin et al. 2010), bottom friction (Hasselmann et al. 1985), and depth-induced breaking (Battjes and Janssen 1978). The only difference between the two domain simulations is the value of the β_{MAX} term defining the strength of the wind input source: for the Atlantic, the β_{MAX} is equal to 1.52; and for the Pacific, it is set at 1.33.

Atlantic and Pacific: The Atlantic and Pacific Ocean simulations use 29 frequency bands, where the starting frequency band is equal to 0.0350 Hz, and follow the equation $f(n+1) = 1.1 \cdot f(n)$. The number of direction bands used is 72 at a resolution of 5°, with a starting direction band of 2.5°.

WIS OPERATIONS: The flowchart in Figure A-1 outlines the WIS 2021 operation procedure. Input files and observational validation data are collected. The simulations are run at one-month segments,

and restart files are built so that temporal consistency is retained between months. QA/QC procedures compare the WIS estimates to the observational validation data before the WIS products are generated and uploaded to the various storage and server locations.

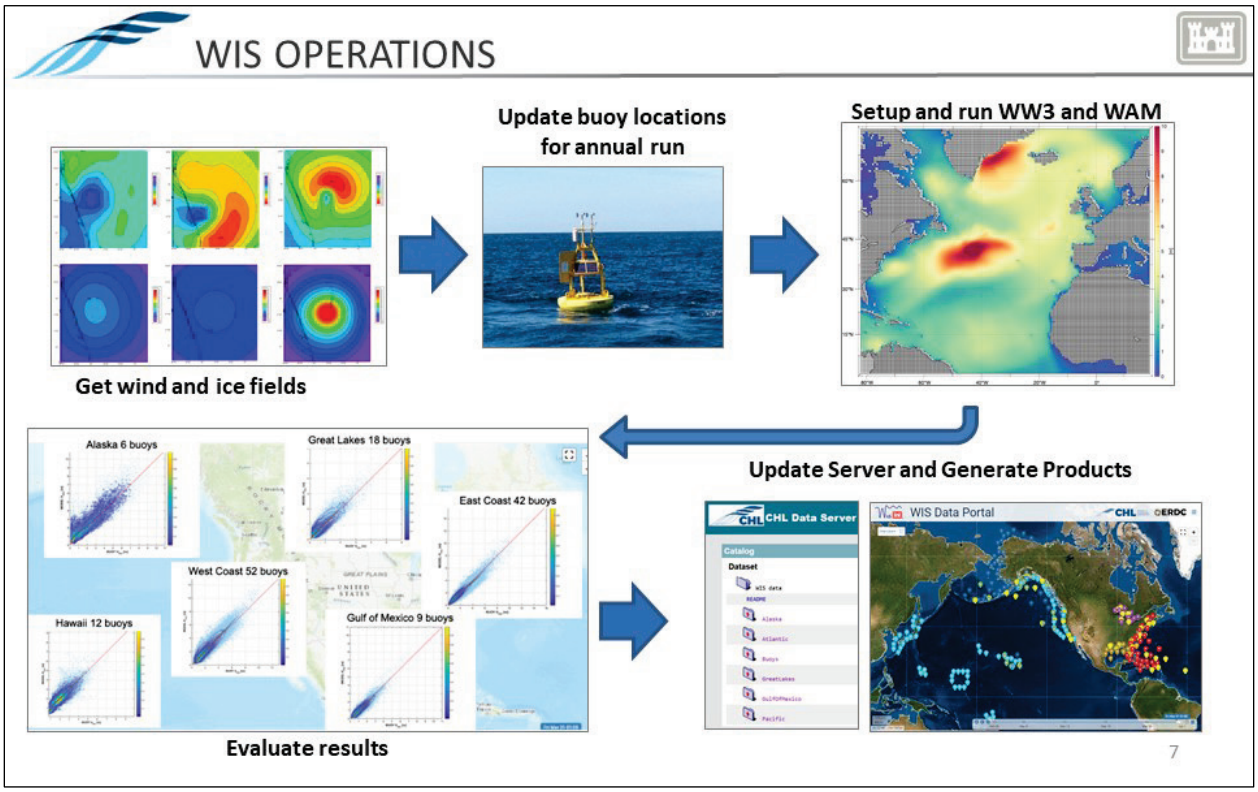

Figure A-1. WIS operations flowchart.

WIS INPUT FILES

Wind and Ice Concentration Fields: All WIS 2021 basins, besides the Great Lakes region, use the ERA5 reanalysis monthly wind and ice files. Oceanweather Inc. (OWI) corrected the wind fields using the top 10 storm events and kinematic procedures on extratropical storms for each designated domain (Cox et al. 1995). ERA5 surface (10 m) winds are marine-exposure and neutral winds at 60 min time intervals (15 min time step during tropical cyclone periods in Hawai'i, Gulf of Mexico, and Atlantic). For all Level 3 (i.e., highest wave model grids, excluding the Southern California Bight) domains, the winds were spatially interpolated from the base resolutions to the wave model grids, as defined in Table A-1. Table A-1 and Figure A-2 also detail the grid extent and data source to be applied for WIS 2021 ERA5 reanalysis product delivery. For the Great Lakes, wind fields are derived from the CFSR (Saha et al. 2010, 2014) database and spatially interpolated to 0.04°, covering the entire domain. Winds are marine-exposure, neutral winds at 60 min time steps.

Alaska and the Great Lakes Ice: For the Alaska model simulations, mean monthly ice concentration fields are used in Level 2 only. The ice concentration fields are derived from the ERA5 database (Hirahara et al. 2016). Implementation of the net effect of ice in WAM is based on a simple approximation, where any open water grid point with a 70% or greater concentration level is set to land. For the Great Lakes, mean daily ice concentration fields are based on work performed by Yang

et al. (2020). Ice concentration fields generally exist for the ice year, defined from December through June of the following year.

Table A-1. WIS 2021 domain information (OWI product delivery, 2022).

Basin	Grid	Extents	Spatial Resolution (deg)	Temporal Resolution (min)	Wind/Pressure Source	Ice	ERA5 Boundary Spectra
Atlantic	Level 1	0 N–75 N 85 W–20 W	0.5	60	ERA5	No	No
Atlantic	Level 2	22 N–48 N 83 W–55 W	0.25	15/60	ERA5 with storm overlay	No	Yes
Gulf of Mexico	Level 2	18 N–31 N 98 W–80 W	0.25	15/60	ERA5 with storm overlay	No	Yes
Pacific	Level 1	64 S–74 N 110 E–300 E	0.5	60	ERA5	No	No
Pacific	Level 2	30 N–50 N 220 E–250 E	0.25	60	ERA5 with storm overlay	No	Yes
Pacific	SOCAL	31.75 N–39.0 N 235 E–243.5 E	0.125	60	ERA5 with storm overlay	No	No
Gulf of Alaska	Arctic	50 N–74 N 155 W–225 W	0.25	60	ERA5 with storm overlay	Yes	Yes
Great Lakes	Basin	41 N–50 N 93.5 W–75.5 W	0.02	60	CFSR	No	No
Hawai'i	Level 2	15.5 N–26 N 163 W–152 W	0.25	15/60	ERA5 with storm overlay	No	Yes

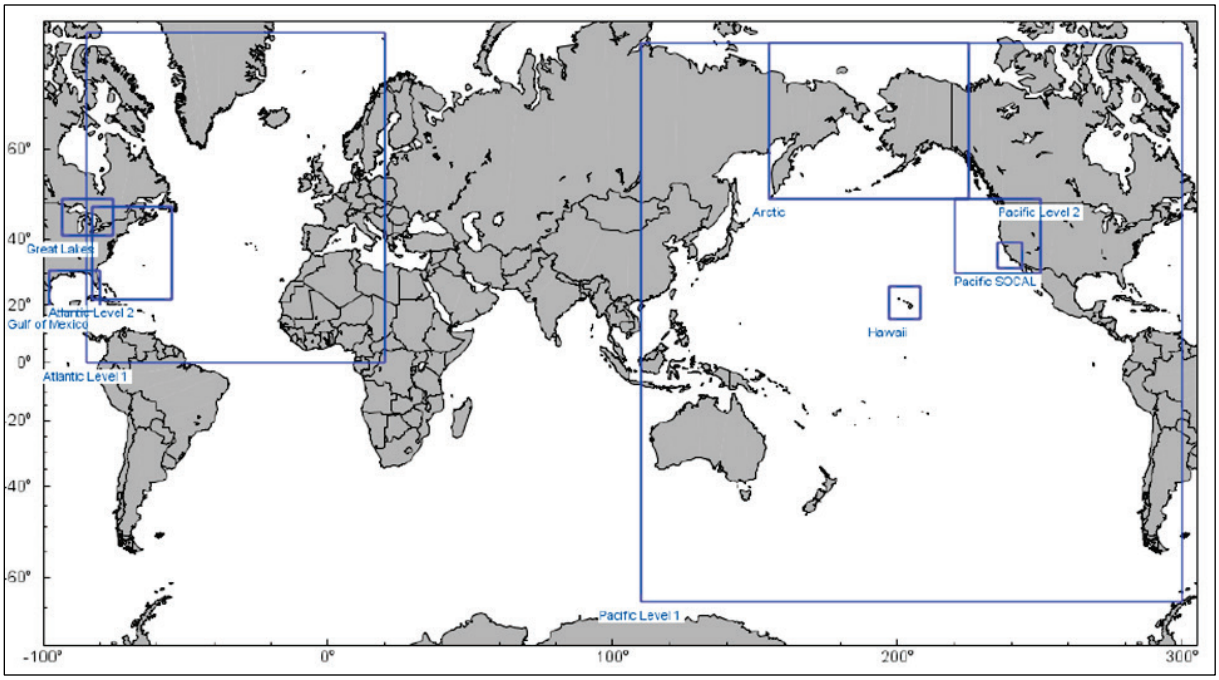

Figure A-2. WIS 2021 domains (OWI product delivery, 2022).

WIS BATHYMETRY AND GRIDS

Bathymetry: For the Atlantic, Gulf of Mexico, Pacific, and Western Alaska, all spherical grids are defined in a spherical coordinate system defined by latitude–longitude pairs. The construction of each domain and level is based on the General Bathymetric Chart of the Oceans (GEBCO 2003). For the near coastal areas, the GEOphysical Data System (GEODAS; National Centers for Environmental Information, n.d.) data are overlaid, replacing the GEBCO results. For the Great Lakes, the grid system for each of the five Great Lakes is based on the Great Lakes Environmental Research Laboratory's digital database (National Centers for Environmental Information, "Great Lakes Bathymetry," n.d.). All model bathymetry grids are defined as the mean low water level.

For the Atlantic, Gulf of Mexico, Pacific, and Western Alaska, grid nesting, where higher resolution grids are nested to minimize computational loads and speed up the simulations, is used. The WIS Atlantic and Gulf of Mexico domains use three levels, with coastal region grid resolutions of 0.083°. The Pacific runs use three primary levels (0.083°), including a refined grid (0.025°) covering the Southern California Bight. Western Alaska uses two levels, where the highest resolution is set at 0.25° to cover the Bering and Chukchi Seas. For the Great Lakes, one grid level is used. Lakes Ontario and Erie are run on a 0.02° model grid, while Lake Huron, Lake Michigan, and Lake Superior model grids are set at 0.04°.

WW3 also uses an obstruction grid that accompanies the actual model grid. The obstruction grid defines subgrid features (e.g., offshore islands) that become directionally dependent, permitting the inclusion of precise sheltering effects that are otherwise omitted.

WIS Evaluations: WIS extensively evaluates modeled wave estimates against point-source measurements and far-field satellite data similar to that of Ortiz-Royero and Mercado-Irizarry (2008), Reguero et al. (2012), Rusu and Guedes Soares (2012), Van Nieuwkoop et al. (2013), Stopa and Cheung (2014), Stopa and Mouche (2017), and Hall and Jensen (2021). WIS estimates require extensive evaluations against all available point-source measurements, including NDBC, CDIP, and MEDS.

For far-field WIS evaluations, data from satellite-borne radar altimeters have been collected and compiled into databases, which are calibrated against buoy data and cross-calibrated against concurrent satellite missions. For the 2021 update evaluation, we used an updated version of the Ribal and Young (2019) database. We paired the altimeter data with the model using altWIZ (Collins and Hesser 2020), which was developed for WIS. In the Pacific, we evaluate the Level 1 Pacific grid and the Level 2 Alaska grid. In the Atlantic, we evaluate the Level 1 Atlantic grid and the Level 2 Gulf of Mexico grid. For each grid, we use data from monthly files of H_{m0} output at every grid point, known as field files. Satellite data cannot currently be applied in the Great Lakes, but improvements to coastal altimeter data may make this feasible in the future. The model data are interpolated to match the altimeter sampling, and statistics are calculated from the paired data.

STATISTICAL EQUATIONS

Bias

$$\text{bias} = \frac{\sum obs - model}{n}.$$

RMSE

$$\text{RMSE} = \sqrt{\frac{\sum(obs - model)^2}{n-1}}.$$

Pearson correlation coefficient

$$\text{corr} = \frac{\sum(obs - \overline{obs})(model - \overline{model})}{\sqrt{\sum(obs - \overline{obs})^2}\sqrt{\sum(model - \overline{model})^2}}.$$

MAE

$$\text{MAE} = \frac{1}{n}\sum_{i=1}^{n}|obs_1 - model_1|.$$

Residual standard error

$$\text{RSE} = \sqrt{\frac{1}{n-2}\sum_{i=1}^{n}(model_\text{i} - obs_1)^2},$$

where

obs = the actual variable (i.e., observational buoy or satellite), and
model = the predicted variable (model: WW3 or WAM).

APPENDIX B: EXAMPLE WIS 2021 INDIVIDUAL SITE EVALUATION PLOTS

Figure B-1 and Figure B-2 show examples of individual site evaluation plots. For the full suite of individual evaluation plots, please contact *WISinfo@usace.army.mil*.

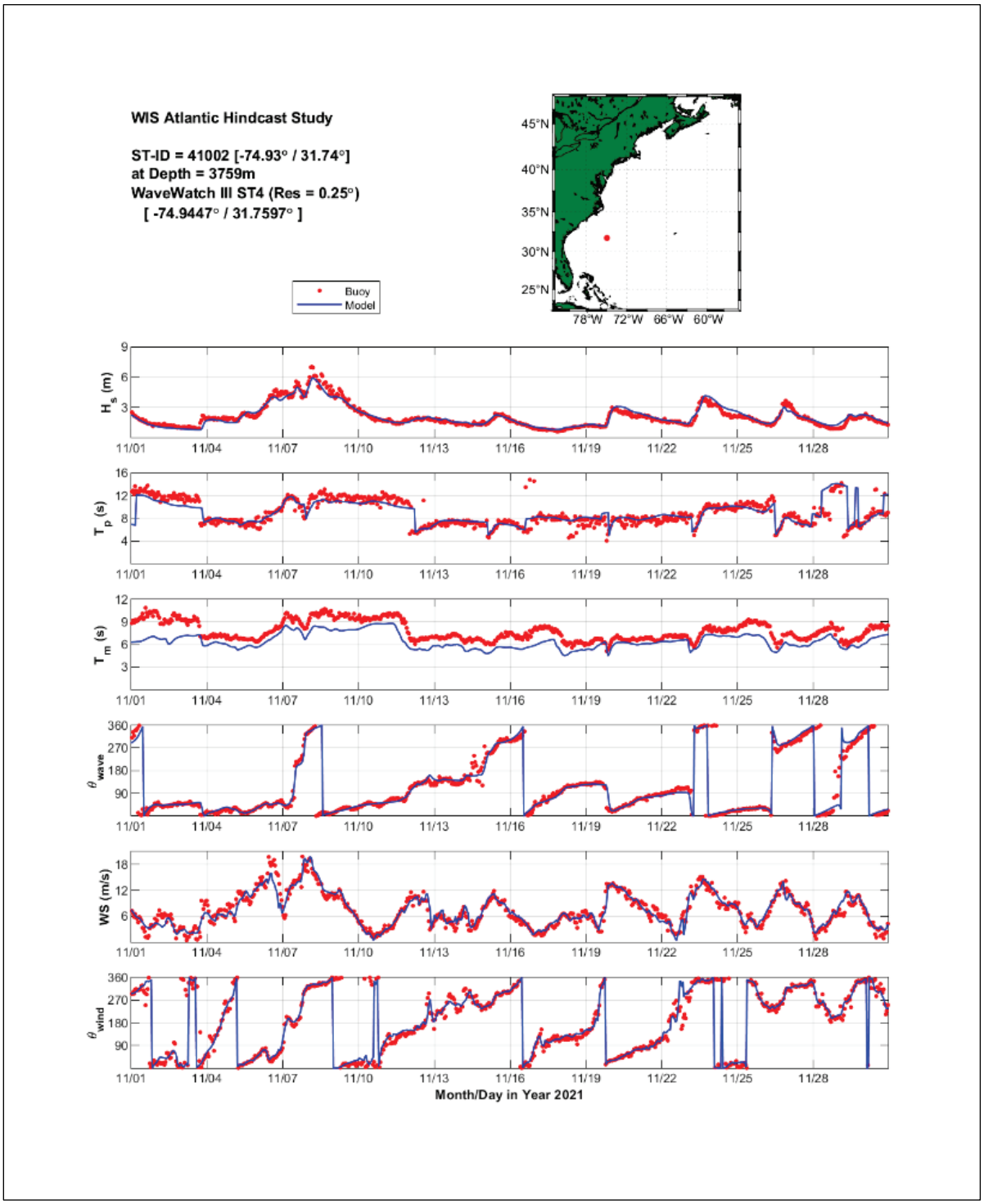

Figure B-1. Example time series plots comparing collocated and concurrent WIS estimates and NDBC 41002 measurements of significant wave height, peak and mean wave periods, mean wave direction at the peak frequency, wind speed, and wind direction.

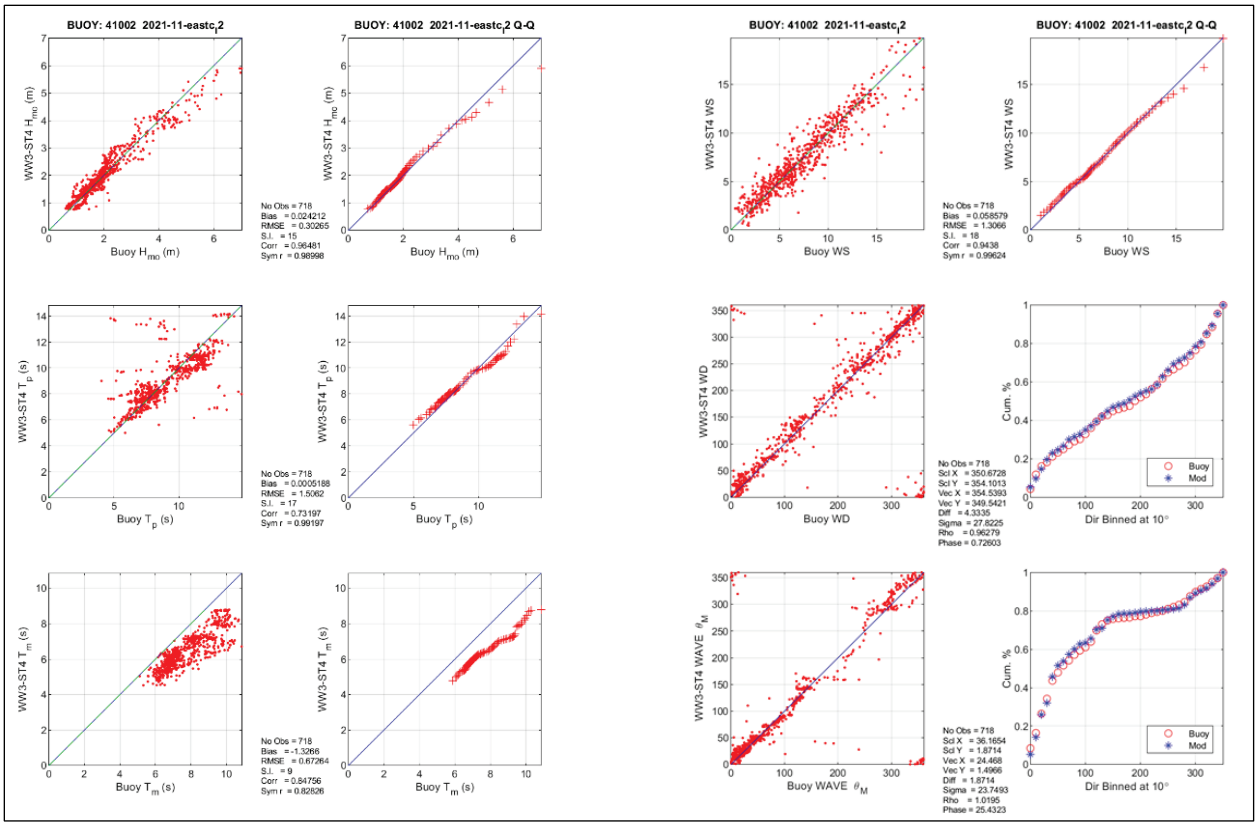

Figure B-2. Example scatter diagrams comparing concurrent and collocated NDBC buoy 41002 measurements against WIS (WW3 model) estimates.